# Neutral and charged exciton fine structure in single lead halide perovskite nanocrystals revealed by magneto-optical spectroscopy

Ming Fu,[†,‡] Philippe Tamarat,[†,‡] He Huang,[§] Jacky Even,[¶] Andrey L. Rogach, [§] and Brahim Lounis[*,†,‡]

[†] *Université de Bordeaux, LP2N, Talence F-33405, France,*

[‡] *Institut d'Optique and CNRS, LP2N, Talence F-33405, France,*

[§] *Department of Physics and Materials Science and Centre for Functional Photonics (CFP), City University of Hong Kong, Kowloon, Hong Kong, SAR China,*

[¶]*Fonctions Optiques pour les Technologies de l'Information, FOTON UMR 6082, CNRS, INSA de Rennes, 35708 Rennes, France*

**E-mail: brahim.lounis@u-bordeaux.fr*

Keywords: Lead halide perovskite, magneto-optical spectroscopy, single nanocrystals, exciton, trion, band-edge fine structure.

## ABSTRACT

*Revealing the crystal structure of lead halide perovskite nanocrystals is essential for the optimization of stability of these emerging materials in applications such as solar cells, photodetectors and light emitting devices. We use magneto-photoluminescence spectroscopy of individual perovskite $CsPbBr_3$ nanocrystals as a unique tool to determine their crystal structure, which imprints distinct signatures in the excitonic sublevels of charge complexes at low temperatures. At zero magnetic field, the identification of two classes of photoluminescence spectra, displaying either two or three sublevels in their exciton fine structure, shows evidence for the existence of two crystalline structures, namely tetragonal $D_{4h}$ and orthorhombic $D_{2h}$ phases. Magnetic field shifts, splitting and coupling of the sublevels provide a determination of the diamagnetic coefficient and valuable information on the exciton g-factor and its anisotropic character. Moreover, this spectroscopic study reveals the optical properties of charged excitons and allows the extraction of the electron and hole g-factors for perovskite systems.*

Lead halide perovskites have proven to be revolutionary semiconductor materials for a new generation of low-cost solar cells.[1-6] In addition to the remarkable photovoltaic performance,[5] such perovskites have high photoluminescence (PL) efficiencies and composition-tunable band gaps, and have been used for perovskite-based light-emitting diodes (LEDs)[7-11], photodetectors[12] and lasers.[13-16] The recent advances in the colloidal synthesis of strongly emitting perovskite nanocrystals (NCs) opens up new possibilities for the fabrication of devices with enhanced performances.[17] Indeed, these materials favorably combine improved optical properties with respect to their bulk counterparts, versatile surface chemistry allowing their dispersion into a variety of solvents and matrices and eventual incorporation into device architectures. Colloidal nanocrystals (NCs) of both methylammonium and cesium lead halides have been recently synthesized with precise size and composition control,[18-23] which opens up opportunities for tunable light sources, such as LEDs[24] and lasers,[25] based on composition and quantum-size tuning[19] and to explore their use as quantum light sources.[26-28] Yet, the intrinsic properties of the emitting states in these materials remain mostly unexplored.

The emission of perovskites at low temperatures stems from the radiative recombination of the band edge exciton which is formed by Coulomb interaction between a hole in one of the S-like valence-band maximum states ($J^h = S^h = 1/2,\ S_z^h = \pm 1/2$), and an electron in one of the two-fold degenerate spin−orbit split-off states ($J^e = 1/2,\ J_z^e = \pm 1/2$).[29,30] A symmetry analysis of the exciton fine structure in the cubic phase predicts an exciton ground state split in a dark state $|0^D\rangle$ with total angular momentum $J^{exc} = 0$ and a triply degenerate bright level with total angular momentum $J^{exc} = 1$ and z projections $J_z^{exc} = 0, \pm 1$.[29,30] For a tetragonal crystal structure, the bright exciton level is split into doubly degenerate bright states $|1^{\pm}\rangle$ ($J^{exc} = 1,\ J_z^{exc} = \pm 1$) and a bright state $|0^B\rangle$ ($J^{exc} = 1,\ J_z^{exc} = 0$).[31,32] Materials with lower crystal structure symmetry, such as orthorhombic phase, should display a further splitting of their fine structure.[33]

It is well known that the crystalline structure of all-inorganic perovskite $CsPbBr_3$ materials depends on the temperature and the growth procedure: An orthorhombic crystallographic phase is usually reported for bulk $CsPbBr_3$ at room temperature, and a series of phase transitions to tetragonal and then to cubic was observed when increasing the temperature.[34,35] The crystal structure is one of the many physical properties that can differ between nanometer-sized and bulk crystalline materials.[36] It also has a major impact on the optical properties of inorganic perovskites[37,38] and thus on their suitability for photovoltaic or light emitting applications. For instance, a metastable cubic phase can be retained in inorganic perovskite nanostructures[6,19] at

room temperature and even down to cryogenic temperatures because of the large contribution of surface energy.[6] Since the energy of the excitonic sublevels is strongly influenced by the crystal structure, magneto-photoluminescence spectroscopy of individual NCs is a unique tool for the identification of the crystalline phase of NCs, as degenerate states can split due to the Zeeman effect and field-induced state-mixing can modify oscillator strengths to reveal hidden "dark" states.[39,40]

In this letter, we report magneto-optical investigations of single inorganic perovskite NCs at liquid helium temperatures, revealing the spectral fingerprint of three bright states assigned to the band-edge exciton. At zero field, the observation of two classes of luminescence spectra, displaying either two or three sublevels in their exciton fine structure, is attributed to the existence of two possible crystalline structures with different degrees of symmetry. Magnetic field shifts, splitting and coupling of the sublevels provides a determination of the diamagnetic coefficient and valuable information on the Landé g-factors and their anisotropic character. Moreover, this spectroscopic study reveals switches of the emission between the exciton multiplet and a red-shifted single line, which splits into two components under magnetic fields. This line is attributed to the recombination of a charged exciton (trion) and its Zeeman splitting allows us to extract the electron and hole g-factors in these systems.

$CsPbBr_3$ NCs with a schematic crystal structure presented in Figure 1a were synthesized by a wet-chemical method[19] (See the Supporting Information for details). Their light absorption spectrum when dissolved in toluene extends from the green excitonic absorption peak at 2.47 eV to the UV range (Figure 1b). Under light excitation at 488 nm, the NCs exhibit a bright green photoluminescence centered at 2.41 eV, with a high color purity (full width at half maximum - FWHM - of 93 meV) and a PL quantum yield exceeding 50% at room temperature. High-resolution transmission electron microscopy (HRTEM) images reveal that they have cubic shapes with average sizes of 8-10 nm (Figure 1c). A cubic perovskite crystal structure at room temperature was refined from X-ray diffraction measurements (see Figure 1d). Previous works[19] on this kind of colloidal NCs reported a cubic crystalline structure while a recent crystallographic study of large (12.5nm) $CsPbBr_3$ NCs at room temperature showed a better refinement of the structure assuming an orthorhombic Pnma space group than with a cubic $Pm3m$[41] space group. However, Bragg diffraction data of smaller (6.5nm) NCs could not be fitted by Rietveld refinement because of extreme peak broadening and increased background signal, and low angle Bragg reflections only

suggest a non-cubic crystal structure.[41] The optical spectroscopy approach described hereafter will allow identifying the crystal structure of perovskite NCs at low temperature.

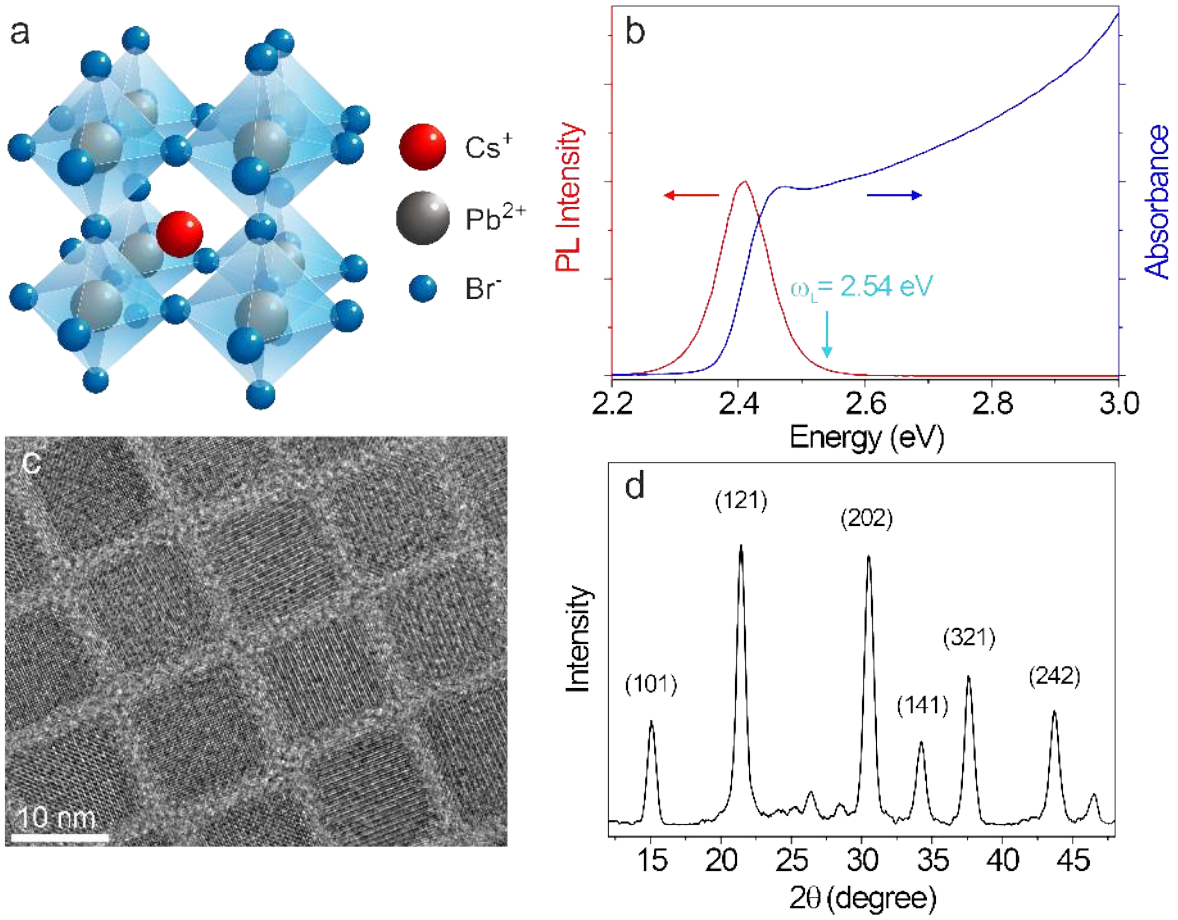


*Figure 1. Basic structural and optical characteristics of $CsPbBr_3$ perovskites NCs. (a), Schematic of the crystal structure of $CsPbBr_3$ perovskites. (b) Absorption (blue) and PL (red) spectra of $CsPbBr_3$ NCs dispersed in toluene. The cyan arrow indicates the excitation wavelength used in our studies. (c) A HRTEM image of $CsPbBr_3$ perovskite NCs. (d) X-ray diffraction pattern of $CsPbBr_3$ perovskite NCs at room temperature.*

A home-built scanning confocal microscope operating at cryogenic temperatures is used to image single NCs deposited by spin-coating on a clean glass coverslip. It is based on a 0.95 numerical aperture objective which is inserted in a magnetic cryostat together with the sample and a piezo-scanner. The objective axis is parallel to the magnetic field, allowing magneto-optical studies in the Faraday configuration. The emitted photons are filtered from the scattered excitation light by a bandpass filter (35 nm FWHM centered on 520 nm) and sent to a single-photon-counting avalanche photodiode and a spectrometer. PL decays are recorded with a conventional time

correlated single-photon-counting setup using a pulsed laser source (optical parametric oscillator at 488 nm, 200 fs pulse width, 80 MHz repetition rate).

Figure 2a shows a representative confocal image of single $CsPbBr_3$ NCs at 2 K under a moderate excitation of 50 $Wcm^{-2}$. The luminescence intensity of most of the single NCs is remarkably stable, as exemplified by the time trace of a single NC presented in Figure 2b. Shot-noise-limited intensity fluctuations could be measured over more than ten seconds of acquisition times. The PL decay of single $CsPbBr_3$ NCs at 2K is monoexponential with a decay time of the order of ~180 ps, as exemplified in Figure 2c, which is similar to that reported for the mixed-halide $CsPb(Cl/Br)_3$ NCs of comparable sizes.[28] The remarkable spectral stability of the NCs at 2K over minutes of integration time (see Figure S1 in the Supporting Information) allows the acquisition of high quality PL spectra, which reveal the band edge exciton fine structure. As displayed in Figure 2d and 2e, the PL spectra at low cw excitation intensities are composed of ultrasharp peaks (with a resolution-limited width ~170μeV) attributed to the exciton recombination zero-phonon-lines (ZPLs). The spectral sharpness of these ZPLs affords the opportunity to investigate subtle differences in the band-edge exciton fine structure from one NC to the other. On the basis of investigations on 57 single NCs, the fine structures of NCs at zero magnetic field can be classified into two types: the type-one (~ 55% of the NCs) is characterized by two ZPLs as displayed in Figure 2d, while the type-two (~ 45% of the NCs) is composed of three ZPLs as displayed in Figure 2e. Interestingly, the temperature dependence of the PL spectrum up to 9 K does not show any evolution of the relative weights of the ZPLs (see Figure S3 in the Supporting Information), which supports an assignment of these lines to recombination lines of bright exciton states having very similar oscillator strengths.[42] The PL spectra also display two phonon replicas which are redshifted by 3.7 meV and 6.3 meV from the ZPLs. These sidebands are attributed to the nearly degenerate first transverse optical (TO) phonon modes.[43] The relative weight of these phonon replicas with respect to the ZPLs is distributed among NCs. For instance, the Huang-Rhys factors for the first and the second optical phonon modes are 0.13 and 0.09 in the case of the NC displayed in Figure 2d, while they are 0.04 and 0.02 for the NC shown in Figure 2e.

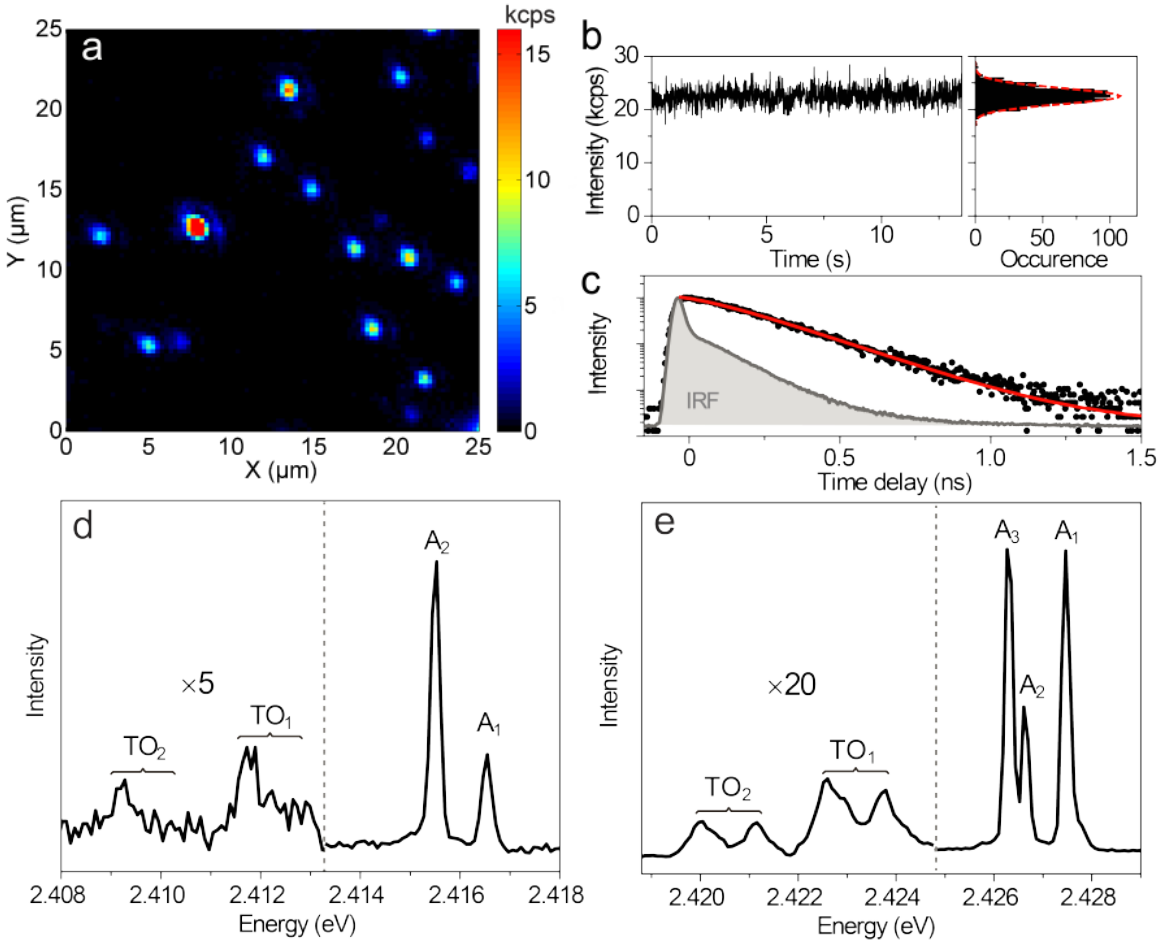


*Figure 2. Spectroscopic characteristics of single $CsPbBr_3$ perovskite NCs at 2 K. (a) Confocal PL image of several single $CsPbBr_3$ NCs dispersed in PMMA at 2 K, excited at 488 nm with a cw intensity of 50 $Wcm^{-2}$. The color bar marks the PL intensity. (b) Time trace of the PL intensity of a single $CsPbBr_3$ NC at 2 K, measured under a 488 nm cw excitation intensity of 50 $Wcm^{-2}$ and with a bin time of 10 ms. The distribution of photon counts per bin is well fitted with a Poisson distribution calculated using the mean number of counts per bin (red curve). (c) Background subtracted PL decay of a single $CsPbBr_3$ NC at 2 K using a 488 nm pulsed excitation with an averaged intensity of 50 $Wcm^{-2}$. The red curve is a mono-exponential fit with a lifetime of ~180 ps. The grey curve corresponds to the instrument response function. (d) PL spectrum of a type-one single $CsPbBr_3$ NC at 2 K recorded over 10 s at an excitation intensity of 50 $Wcm^{-2}$. (e) PL spectrum of a type-two single $CsPbBr_3$ NC at 2 K recorded over 1 min at an excitation intensity of 50 $Wcm^{-2}$. The peaks labeled $A_i$ are attributed to the ZPLs of bright exciton fine structure states. The peaks $TO_j$ are assigned to the $j^{th}$ transverse optical phonon sidebands of the ZPLs. The PL intensities of all lines have a linear dependence on the excitation intensity at these levels of excitations (see Figure S2), excluding any biexcitonic origin.*

To gain a deeper insight into the NCs band-edge exciton fine structure, we studied their magneto-optical properties. Figure 3a exemplifies the evolution of the PL spectrum of a type-one single NC as a function of the magnetic field amplitude. The well-resolved Zeeman splitting of the

higher energy line corresponds to the Faraday configuration where a symmetry axis of the NC is oriented along the magnetic field. This is a hallmark of the $D_{4h}$ point group symmetry corresponding to the P4/mbm crystallographic phase, which has previously been identified only in bulk $CsPbBr_3$ at high temperature.[34] Following the effective mass model of band-edge exciton in a uniaxial crystal structure[31,32,44] and taking the crystal axis along z, the type-one spectroscopic behavior suggests the attribution of the zero-field higher energy line to the doubly degenerate bright exciton sublevel $|1^{\pm}\rangle$, while the lower energy line is assigned to the non-degenerate bright exciton sublevel $|0^{B}\rangle$. It should be noted that in a minority of cases, we found an inversion of level ordering between both bright sub-levels.

Zeeman splittings of the bright level $|1^{\pm}\rangle$ were measured on 17 single NCs, with the data showing an evidence for a strong anisotropy of the exciton Landé in these NCs. The distribution of the values of $g_{\parallel}^{exc}\cos\theta$ ($\theta$ being the angle between the magnetic field and the NC z axis) is presented in Figure 3b and points to two sub-populations of NCs. Most of the NCs (12 over 17) such as the one exemplified in Figure 3c, do not display measurable Zeeman splitting, while 5 NCs, such as the one exemplified in Figure 3a, display a $g_{\parallel}^{exc}\cos\theta$ up to 2. We deduce that the latter NCs have their z axis nearly parallel to the magnetic field and therefore estimate $g_{\parallel}^{exc} \sim 2$, where $g_{\parallel}^{exc} = g_{\parallel}^{e} + g_{\parallel}^{h}$, $g^{e}$ and $g^{h}$ being the electron and hole g-factors,[44] respectively. Besides the linear Zeeman splitting, the $|1^{\pm}\rangle$ states display clear diamagnetic shifts with a diamagnetic coefficient of the order of a few $\mu eV\, T^{-2}$, in accordance with previous determinations in hybrid organic-inorganic lead-halide-based perovskite crystals.[29,45]

According to effective mass models, a magnetic field parallel to the z crystal axis should also induce a coupling between the $|0^{B}\rangle$ bright state and the lowest energy dark state $|0^{D}\rangle$.[31,44] No signature of a magnetic brightening of the dark state or lowering of PL intensity of the bright state was observed in our experiments where magnetic fields are limited to 7T. We also probed the relaxation dynamics of single NCs with and without application of magnetic field. A representative example of PL decay is displayed in Figure 3d for the same NC as in Figure 3a. It has a monoexponential behavior with a lifetime of ~200 ps, regardless of the magnetic field. This suggests that decays are imposed by fast non-radiative relaxation processes which dominate the exciton radiative recombination.

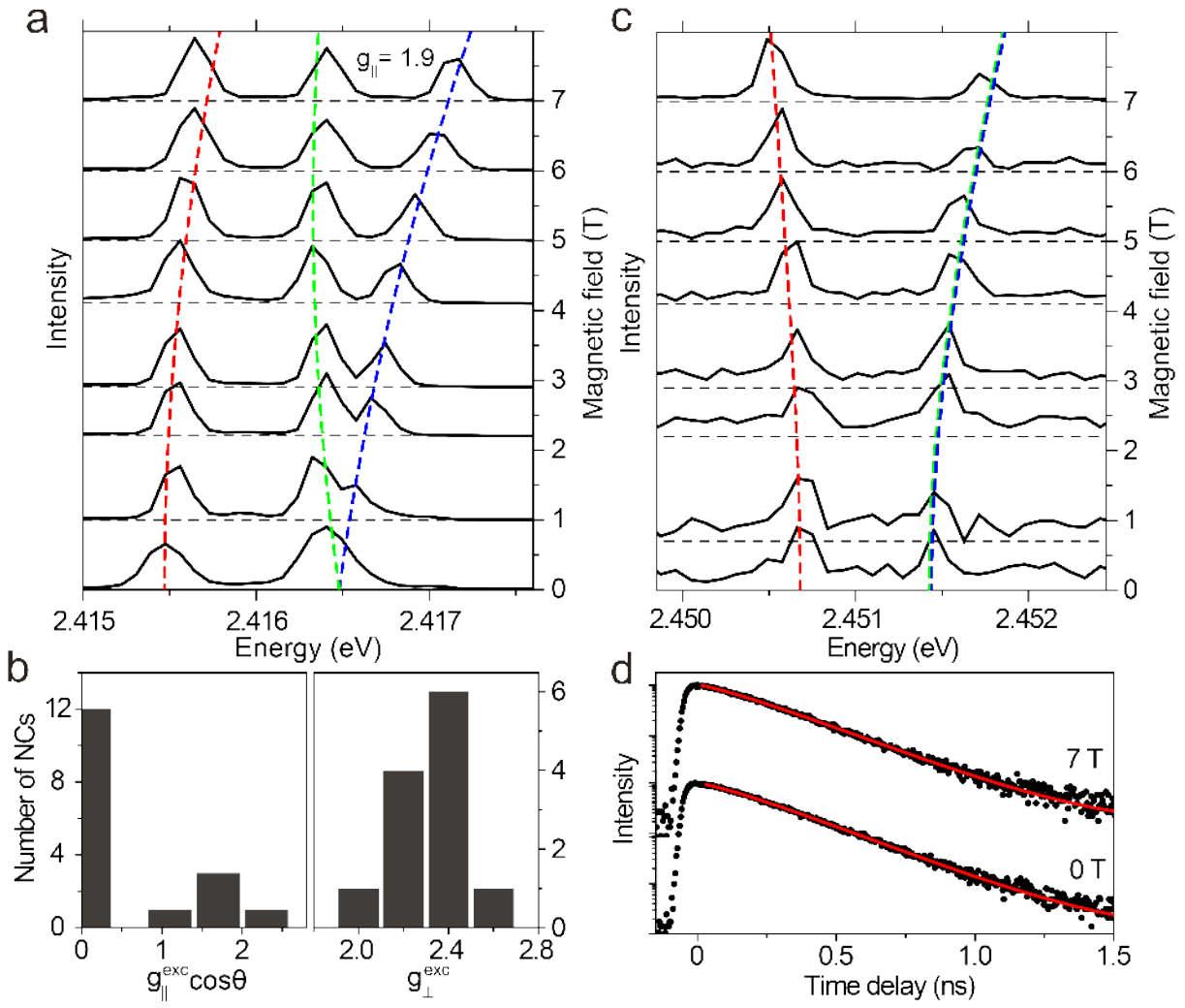


*Figure 3. Magneto-optical properties of type-one NCs. (a) Evolution of the PL spectrum of a NC under magnetic fields ranging from 0 to 7 T. A linear fit of the Zeeman splitting of the high-energy ZPL yields* $g_{\parallel}^{exc} = 1.9$. *(b) Left: Histogram of* $g_{\parallel}^{exc}\cos\theta$ *for 17 NCs. For the 12 NCs showing no Zeeman splitting, the orthogonal g-factor is extracted from* $g_{\perp}^{exc} = \sqrt{\Delta^2 - \Delta_0^2}/(\mu_B B)$ *and displayed in the right histogram. (c) Evolution of the PL spectrum under magnetic fields of another NC, for which* $g_{\parallel}^{exc} = 0$. *(d) PL decays of the same* $CsPbBr_3$ *NC at 0 T and at 7 T, under 488 nm excitation with averaged intensity of 50* $Wcm^{-2}$. *The decays are fitted by mono-exponential curves with lifetimes of ~200 ps.*

NCs which do not display Zeeman splitting have their crystal axis z orthogonal to the magnetic field and undergo a magnetic coupling between the $|0^B\rangle$ bright state and the combination state $|\psi_+\rangle = (|1^+\rangle + |1^-\rangle)/\sqrt{2}$ with a coupling strength $\left(g_{\perp}^{e} + g_{\perp}^{h}\right)\mu_B B/2$, while the $|0^D\rangle$ dark state is coupled to $|\psi_-\rangle = (|1^+\rangle - |1^-\rangle)/\sqrt{2}$ with a coupling strength $\left(g_{\perp}^{e} - g_{\perp}^{h}\right)\mu_B B/2$.[31,44] As exemplified in Figure 3c, the state mixing is accompanied by a quadratic shift of the ZPLs but no

degeneracy lifting of $|\psi_+\rangle$ and $|\psi_-\rangle$ is observed under magnetic field. Since the energy position of the dark state could not be extracted from the spectra, we could not access to $g_\perp^e - g_\perp^h$. Nevertheless, one can estimate the orthogonal exciton g-factor $g_\perp^{exc} = g_\perp^e + g_\perp^h$ using the field evolution of the ZPLs spectral positions corresponding to the eigen-energies of the $\{|0^B\rangle, |\psi_+\rangle\}$ coupled system. For the 12 NCs with no Zeeman splittings we obtain a $g_\perp^{exc}$ distribution centered around ~2.3 (see Figure 3b). Overall, the values of $g_\perp^{exc}$ and $g_\parallel^{exc}$ extracted from this magneto-PL of the exciton are in accordance with the numerical values of $g^{exc} = g^e + g^h$ deduced from the effective mass model.[44] A separate determination of $g^e$ and $g^h$ for each NC would require further investigations of the magnetic field effect on the energy structure of other charge complexes such as charged excitons. This point will be discussed further below.

We now discuss the magneto-PL properties of the type-two NCs, having a fine structure composed of three ZPLs in zero-field. The NC of Figure 4a shows a fine structure where the higher and the lower energy lines have pure linear and orthogonal polarizations in zero field, while they become circularly polarized with opposite helicities at 7 T. As schematically depicted in Figure 4c, the symmetry lowering is the dominant effect in zero field and lifts the $|1^\pm\rangle$ bright states degeneracy, producing two split states with linear and orthogonal dipoles. At high magnetic field, where the Zeeman splitting becomes larger than the zero-field splitting, the eigenstates tend toward genuine $|1^\pm\rangle$ states with circular right and left polarizations. The mid-energy line has no clear circular polarization character at 7T and is attributed to a bright state with a transition dipole moment parallel to the magnetic field. This behavior recalls similar observations in self-assembled semiconductor quantum dots[46,47] and colloidal NCs[48,49] expressing pronounced quantum confinement effects, where symmetry breaking by shape anisotropy leads to a lift of a fine structure degeneracy (see Figure 4c). Since our perovskite NCs have a size larger than the exciton Bohr diameter (~7nm)[19,50] shape effects can be neglected. Type-two NCs are thus attributed to NCs having an orthorhombic crystal structure with a reduced $D_{2h}$ point symmetry compared to that of type-one NCs ($D_{4h}$). This crystal structure is consistent with the Pnma crystallographic phase observed in bulk $CsPbBr_3$ at room temperature.[34] It should be noted that the pure polarization character of the lines displayed in Figure 4 was observed on only 1 over 7 studied NCs, since this behavior requires that the broken NC symmetry axis be along the direction of the magnetic field. Similar but partial polarization signatures were observed on all other type-two NCs, reflecting the random orientation of the NCs with respect to the magnetic field.

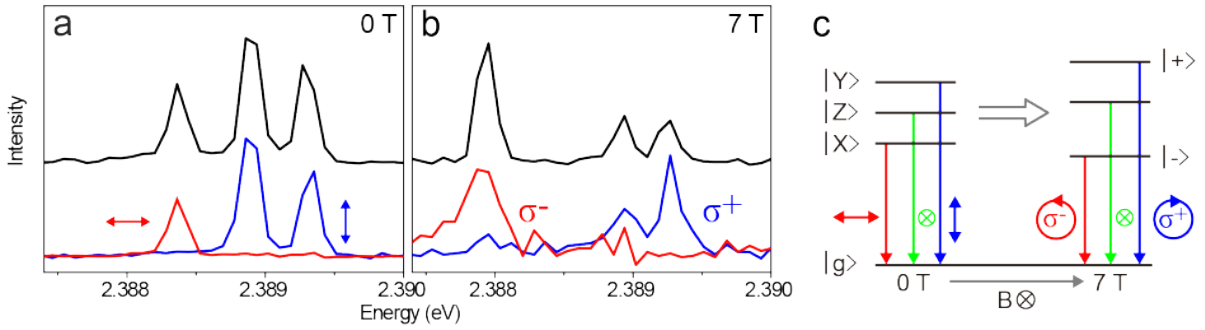


*Figure 4. Polarization analysis of the PL spectral components of a type-two NC under magnetic fields. The black lines correspond to the PL spectrum of a single NC under zero field (a) and 7 T (b). At 0 T, the horizontally (resp. vertically) polarized PL shows a strong horizontal (resp. vertical) polarization for the lowest (resp. highest) energy ZPL. At 7T, the circularly polarized $\sigma^+$ (resp. $\sigma^-$) PL shows a strong $\sigma^+$ (resp. $\sigma^-$) polarization for the lowest (resp. highest) energy ZPL. The central ZPL has no clear polarization under magnetic fields. (c) Scheme of Zeeman splitting and polarization properties of a bright exciton doublet displaying an intrinsic linearly polarized XY fine structure in zero field.*

Symmetry considerations provide solid foundations for the attribution of type-one and type-two fine structures to tetragonal ($D_{4h}$) or orthorhombic ($D_{2h}$) crystal structures, respectively. In the Supporting Information we describe the exciton fine structure using a Frenkel picture, as reported previously for 2D[31,32] or 3D[44] uniaxial systems ($D_{4h}$ or $C_{4v}$) in the hybrid inorganic-organic lead halide perovskites. To take into account the reduction of the lattice point symmetry to $D_{2h}$ in the orthorhombic crystal structure, we start from the $D_{4h}$ basis functions and add to the Hamiltonian coupling terms introduced by the additional crystal field (see the Supporting Information). This leads to four non-degenerate exciton states, one dark state and three optically active ones having orthogonal transition dipole moments, oriented along the three crystal axes (see Figure S6 in the Supporting Information).

Another important finding with $CsPbBr_3$ NCs studied here is the magneto-optical spectroscopic signature of the charged exciton (trion). Most of the studied NCs (~60%) have their emission switching between the multiline excitonic fine-structure and a red-shifted single ZPL named X* (with a resolution-limited width), as exemplified in Figure 5a (see also Figure S4 in the Supporting Information). The distribution of spectral shifts between the lowest-energy fine structure ZPL and the X* ZPL ranges from 6 to 24 meV, as shown in the histogram of Figure 5b. Similar spectral jumps in the low temperature PL spectra of single colloidal mixed-halide $CsPb(Cl/Br)_3$ and $CsPbI_3$ NCs were recently reported.[28,51] A trion state could for instance be formed when an exciton is created in the presence of an unpaired charge carrier in the core of the NC and a

charge carrier trapped at its surface or in a lattice defect. Interestingly, the integrated intensities of the exciton and trion lines are very similar in these NCs, meaning that the quantum yield of these two charge complexes are comparable. For one NC which spent sufficiently long residence times (few tens of seconds) in neutral or charged states, we could even record separately the PL decay of the exciton and trion and found that they are monoexponential with characteristic lifetimes of 270 ps and 320 ps respectively (see Figure S5 in the Supporting Information). Since radiative recombination of the trions is expected to be twice faster than that of excitons,[52] these measurements confirm that the non-radiative processes are dominant in the relaxation of the charge complexes in these systems at low temperatures.

Charged NCs serve as the ideal system to investigate single charge-carrier spin properties, in particular to directly measure both $g^e$ and $g^h$ using magneto-optical spectroscopy.[47,53,54] Indeed, in a charged NC, the angular momentum of the ground state is set by the extra-charge carrier, while the trion's one is given by the opposite charge carrier. Therefore, the angular momentum of a positively (resp. negatively) charged NC in the ground state is that of the hole (resp. electron) spin. Under an external magnetic field, the energy splitting of the ground state is thus $\Delta_h = g^h \mu_B B$ (resp. $\Delta_e = g^e \mu_B B$). After a photon absorption and the generation of an extra e-h pair in the NC, a trion is created. Due to the pairing of the two holes (resp. two electrons), the lowest-energy eigenstates of the trion form a doublet having a total angular momentum set by that of the unpaired electron (resp. hole). Under magnetic fields, the trion state splitting is therefore $\Delta_e = g^e \mu_B B$ (resp. $\Delta_h = g^h \mu_B B$). As presented in Figure 5c for the case of a positive trion, the trion recombination generally presents four transitions that are shifted in energy by $(\pm g^e \pm g^h)\mu_B B$ from the zero-field line.[47,53] We could perform magneto-PL spectroscopy of trions on 14 individual NCs (6 of type-one and 8 of type-two) and found that all X* lines display a two-line Zeeman splitting, as exemplified in Figure 5d. The narrow distribution of the trion recombination g-factors presented in Figure 5e is centered on ~2.4 for both types of NCs and points to a nearly isotropic character of the magnetic response of the charged NCs. There are two possible situations leading to the observation of a Zeeman doublet: the first one requires that two of the four transitions are forbidden, which is expected for NCs with a $D_{4h}$ symmetry and a z axis oriented parallel to the magnetic field; the second one implies that $g_e$ or $g_h$ is close to zero. Our findings support the second assumption since NCs are unlikely to be all oriented along the magnetic field. Indeed, for type-one NCs, the isotropic trion recombination g-factor is compatible with the calculations of $g_e$ and $g_h$ derived from effective mass calculations for

hybrid inorganic-organic lead halide perovskites uniaxial systems,[44] $g_h$ being much smaller than $g_e$.

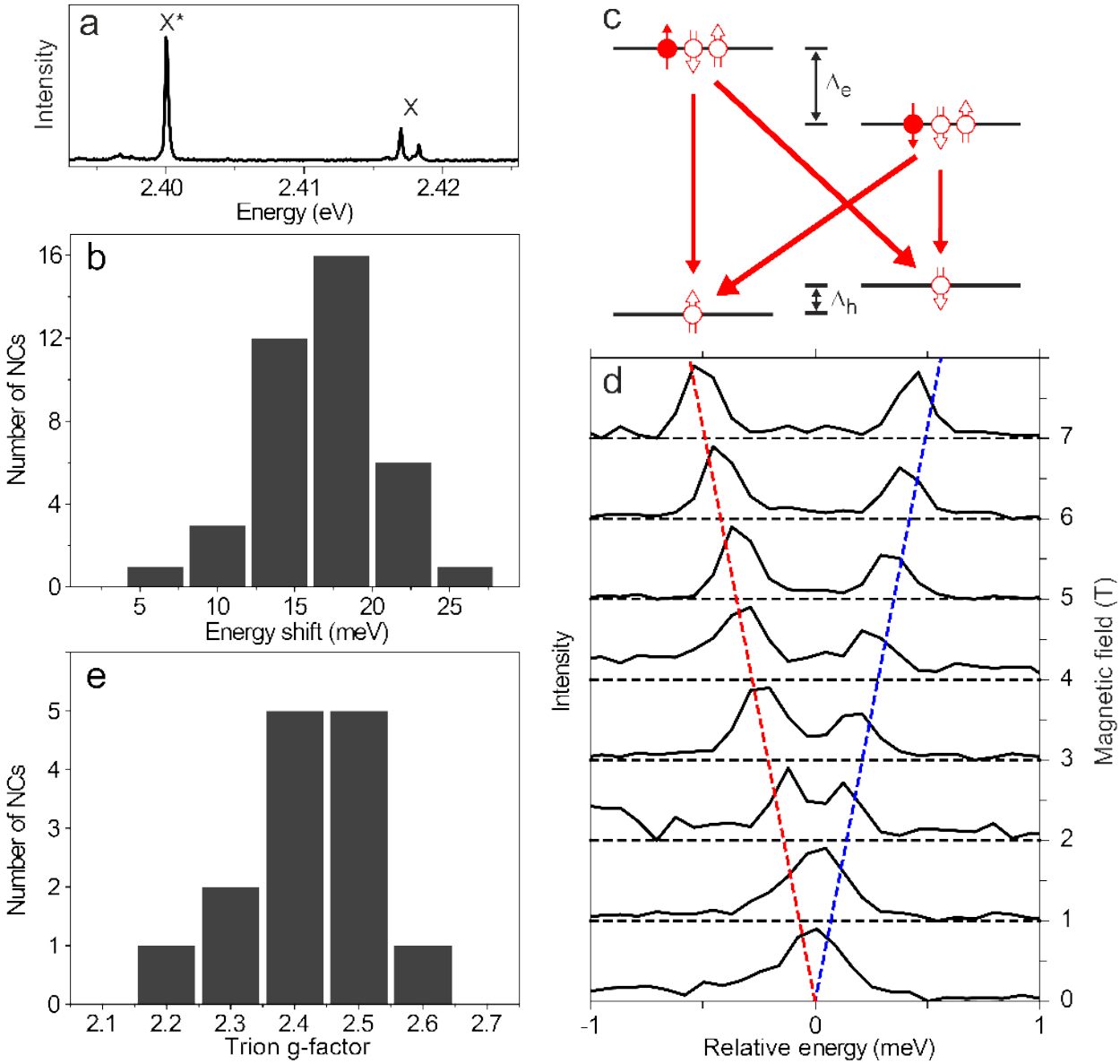


*Figure 5. Optical properties of trion states at 2K. (a) PL spectra of a single $CsPbBr_3$ NC, recorded over 1 s at an excitation of 50 $Wcm^{-2}$. The X structure arises from the neutral exciton fine structure, while the X* line is attributed to a trion recombination. (b) Histogram of the spectral shift between the peak X* and the lowest energy peak of the X structure, for 39 single NCs. (c) Recombination scheme for a positive trion under a magnetic field with a hole level splitting $\Delta_h$ smaller than the electron splitting $\Delta_e$. (d) Zeeman splitting of the X* line, yielding the trion g-factor $g^{trion} = 2.4$. (e) Histogram of trion g-factors for 14 NCs.*

In conclusion, magneto-PL studies provide spectroscopic signatures of charge complexes states in inorganic lead halide perovskite NCs which reveal two distinct crystalline structures existing at liquid helium temperatures, an information that could hardly be extracted by other methods. Two-line and three-line fine structure emissions at zero magnetic field are the hallmarks of tetragonal and orthorhombic phases of the NCs, respectively. Altogether, this first derivation of the exciton and trion Landé factors indicates that in these perovskites the electron g-factor is close to that of free electrons ($g^e \sim 2$), while the hole g-factor is much smaller ($|g^h| \lesssim 0.4$). These spectroscopic findings will guide the development of accurate theoretical models and help to improve the understanding of magnetic field effects on the spin-dependent generation and recombination processes in perovskite-based materials.[54] An open question raised by our work concerns the position of the dark state level with respect to the bright levels, and the relaxation rates to and from this level. Further investigations will also aim at determining the optical coherence lifetime of the emission lines in these NCs, in order to probe their potential for new applications in quantum optics technologies.

Supporting Information:
The Supporting Information is available free of charge via the Internet at http://pubs.acs.org.
Details on the sample preparation and characterization, supplementary experimental data on the spectral stability of the NCs, the dependence of their PL intensity on the excitation intensity, the temperature dependence of the PL spectrum, the spectral trajectories of the exciton lines and the trion lines, emission properties of the same single NC in neutral and charged states under a magnetic field of 7T, as well as symmetry considerations on the exciton fine structure.

**Acknowledgement**

We thank Xiaoyong Wang for fruitful discussions at the early stage of this work. We acknowledge the financial support from the French National Agency for Research, Région Aquitaine, Idex Bordeaux (LAPHIA Program), the French Ministry of Education and Research and the Institut universitaire de France, and from the Research Grant Council of Hong Kong S.A.R. (GRF project CityU 11337616).

**References**


(1) Kojima, A.; Teshima, K.; Shirai, Y.; Miyasaka, T. *J. Am. Chem. Soc.* **2009**, *131*, 6050–6051.
(2) Green, M. A.; Ho-Baillie, A.; Snaith, H. J. *Nat. Phys.* **2014**, *8*, 506–514.
(3) Zhou, H.; Chen, Q.; Li, G.; Luo, S.; Song, T.-B.; Duan, H.-S.; Hong, Z.; You, J.; Liu, Y.; Yang, Y. *Science* **2014**, *345*, 542–545.
(4) McMeekin, D. P.; Sadoughi, G.; Rehman, W.; Eperon, G. E.; Saliba, M.; Haghighirad, A.; Hörantner, M. T.; Sakai, N.; Korte, L.; Rech, B.; Johnston, M. B.; Herz, L. M.; Snaith, H. J. *Science* **2016**, *351*, 151–155.
(5) Zhou, Y.; Zhu, K. *ACS Energy Lett.* **2016**, *1*, 64–67.
(6) Swarnkar, A.; Marshall, A. R.; Sanehira, E. M. *Science* **2016**, *354*, 92–95.
(7) Tan, Z.-K.; Moghaddam, R. S.; Lai, M. L.; Docampo, P.; Higler, R.; Deschler, F.; Price, M.; Sadhanala, A.; Pazos, L. M.; Credgington, D.; Hanusch, F.; Bein, T.; Snaith, H. J.; Friend, R. H. *Nat. Mater.* **2014**, *9*, 687–692.
(8) Li, G.; Tan, Z.-K.; Di, D.; Lai, M. L.; Jiang, L.; Lim, J. H.-W.; Friend, R. H.; Greenham, N. C. *Nano Lett.* **2015**, *15*, 2640–2644.
(9) Kim, Y.-H.; Cho, H.; Heo, J. H.; Kim, T.-S.; Myoung, N.; Lee, C.-L.; Im, S. H.; Lee, T.-W. *Adv. Mater.* **2015**, *27*, 1248–1254.
(10) Zhang, X.; Lin, H.; Huang, H.; Reckmeier, C.; Zhang, Y.; Choy, W. C. H.; Rogach, A. L. *Nano Lett.* **2016**, *16*, 1415–1420.
(11) Sutherland, B. R.; Sargent, E. H. *Nat. Phys.* **2016**, *10*, 295–302.
(12) Zhu, H. L.; Cheng, J.; Zhang, D.; Liang, C.; Reckmeier, C. J.; Huang, H.; Rogach, A. L.; Choy, W. C. H. *ACS Nano* **2016**, *10*, 6808–6815.
(13) Xing, G.; Mathews, N.; Lim, S. S.; Yantara, N.; Liu, X.; Sabba, D.; Grätzel, M.; Mhaisalkar, S.; Sum, T. C. *Nat. Mater.* **2014**, *13*, 476–480.
(14) Zhu, H.; Fu, Y.; Meng, F.; Wu, X.; Gong, Z.; Ding, Q.; Gustafsson, M. V.; Trinh, M. T.; Jin, S.; Zhu, X.-Y. *Nat. Mater.* **2015**, *14*, 636–642.
(15) Xing, J.; Liu, X. F.; Zhang, Q.; Ha, S. T.; Yuan, Y. W.; Shen, C.; Sum, T. C.; Xiong, Q. *Nano Lett.* **2015**, *15*, 4571–4577.
(16) Xu, Y.; Chen, Q.; Zhang, C.; Wang, R.; Wu, H.; Zhang, X.; Xing, G.; Yu, W. W.; Wang, X.; Zhang, Y.; Xiao, M. *J. Am. Chem. Soc.* **2016**, *138*, 3761–3768.
(17) Huang, H.; Polavarapu, L.; Sichert, J. A.; Susha, A. S.; Urban, A. S.; Rogach, A. L. *NPG Asia Materials* **2016**, *8*, e328.
(18) Schmidt, L. C.; Pertegás, A.; González-Carrero, S.; Malinkiewicz, O.; Agouram, S.; Mínguez Espallargas, G.; Bolink, H. J.; Galian, R. E.; Pérez-Prieto, J. *J. Am. Chem. Soc.* **2014**, *136*, 850–853.
(19) Protesescu, L.; Yakunin, S.; Bodnarchuk, M. I.; Krieg, F.; Caputo, R.; Hendon, C. H.; Yang, R. X.; Walsh, A.; Kovalenko, M. V. *Nano Lett.* **2015**, *15*, 3692–3696.
(20) Zhang, F.; Zhong, H.; Chen, C.; Wu, X.-G.; Hu, X.; Huang, H.; Han, J.; Zou, B.; Dong, Y. *ACS Nano* **2015**, *9*, 4533–4542.
(21) Huang, H.; Susha, A. S.; Kershaw, S. V.; Hung, T. F.; Rogach, A. L. *Adv. Sci.* **2015**, *2*, 1500194.
(22) Huang, H.; Chen, B.; Wang, Z.; Hung, T. F.; Susha, A. S.; Zhong, H.; Rogach, A. L. *Chem. Sci.* **2016**, *7*, 5699–5703.
(23) Tong, Y.; Bladt, E.; Aygüler, M. F.; Manzi, A.; Milowska, K. Z.; Hintermayr, V. A.; Docampo, P.; Bals, S.; Urban, A. S.; Polavarapu, L.; Feldmann, J. *Angew. Chem.* **2016**, *128*, 14091–14096.

(24) Song, J.; Li, J.; Li, X.; Xu, L.; Dong, Y.; Zeng, H. *Adv. Mater.* **2015**, *27*, 7162–7167.
(25) Wang, Y.; Li, X.; Song, J.; Xiao, L.; Zeng, H.; Sun, H. *Adv. Mater.* **2015**, *27*, 7101–7108.
(26) Park, Y.-S.; Guo, S.; Makarov, N. S.; Klimov, V. I. *ACS Nano* **2015**, *9*, 10386–10393.
(27) Hu, F.; Zhang, H.; Sun, C.; Yin, C.; Lv, B.; Zhang, C.; Yu, W. W.; Wang, X.; Zhang, Y.; Xiao, M. *ACS Nano* **2015**, *9*, 12410–12416.
(28) Rainò, G.; Nedelcu, G.; Protesescu, L.; Bodnarchuk, M. I.; Kovalenko, M. V.; Mahrt, R. F.; Stöferle, T. *ACS Nano* **2016**, *10*, 2485–2490.
(29) Tanaka, K.; Takahashi, T.; Ban, T.; Kondo, T.; Uchida, K.; Miura, N. *Solid State Commun.* **2003**, *127*, 619–623.
(30) Even, J. *J. Phys. Chem. Lett.* **2015**, *6*, 2238–2242.
(31) Kataoka, T.; Kondo, T.; Ito, R.; Sasaki, S.; Uchida, K.; Miura, N. *Phys. Rev. B* **1993**, *47*, 2010–2018.
(32) Tanaka, K.; Takahashi, T.; Kondo, T.; Umeda, K.; Ema, K.; Umebayashi, T.; Asai, K.; Uchida, K.; Miura, N. *Jpn. J. Appl. Phys.* **2005**, *44*, 5923–5932.
(33) Karlsson, K. F.; Dupertuis, M. A.; Oberli, D. Y.; Pelucchi, E.; Rudra, A.; Holtz, P. O.; Kapon, E. *Phys. Rev. B* **2010**, *81*, 161307.
(34) Hirotsu, S.; Harada, J.; Iizumi, M.; Gesi, K. *J. Phys. Soc. Jpn.* **1974**, *37*, 1393–1398.
(35) Stoumpos, C. C.; Malliakas, C. D.; Peters, J. A.; Liu, Z.; Sebastian, M.; Im, J.; Chasapis, T. C.; Wibowo, A. C.; Chung, D. Y.; Freeman, A. J.; Wessels, B. W.; Kanatzidis, M. G. *Cryst. Growth Des.* **2013**, *13*, 2722–2727.
(36) Alivisatos, A. P. *Science* **1996**, *271*, 933–937.
(37) Eperon, G. E.; Paternò, G. M.; Sutton, R. J.; Zampetti, A.; Haghighirad, A. A.; Cacialli, F.; Snaith, H. J. *J. Mater. Chem. A* **2015**, *3*, 19688–19695.
(38) Grancini, G.; Marras, S.; Prato, M.; Giannini, C.; Quarti, C.; De Angelis, F.; De Bastiani, M.; Eperon, G. E.; Snaith, H. J.; Manna, L.; Petrozza, A. *J. Phys. Chem. Lett.* **2014**, *5*, 3836–3842.
(39) Nirmal, M.; Norris, D. J.; Kuno, M.; Bawendi, M. G.; Efros, A. L.; Rosen, M. *Phys. Rev. Lett.* **1995**, *75*, 3728–3731.
(40) Fernée, M. J.; Tamarat, P.; Lounis, B. *Chem. Soc. Rev.* **2014**, *43*, 1311.
(41) Cottingham, P.; Brutchey, R. L. *Chem.Commun.* **2016**, *52*, 5246–5249.
(42) Fernée, M. J.; Tamarat, P.; Lounis, B. *J. Phys. Chem. Lett.* **2013**, *4*, 609–618.
(43) Calistru, D. M.; Mihut, L.; Lefrant, S.; Baltog, I. *J. Appl. Phys.* **1997**, *82*, 5391.
(44) Yu, Z. G. *Sci. Rep.* **2016**, *6*, 28576.
(45) Hirasawa, M.; Ishihara, T.; Goto, T.; Uchida, K.; Miura, N. *Physica B: Condensed Matter* **1994**, *201*, 427–430.
(46) Bayer, M.; Kuther, A.; Forchel, A.; Gorbunov, A.; Timofeev, V. B.; Schäfer, F.; Reithmaier, J. P.; Reinecke, T. L.; Walck, S. N. *Phys. Rev. Lett.* **1999**, *82*, 1748–1751.
(47) Bayer, M.; Ortner, G.; Stern, O.; Kuther, A.; Gorbunov, A. A.; Forchel, A.; Hawrylak, P.; Fafard, S.; Hinzer, K.; Reinecke, T. L.; Walck, S. N.; Reithmaier, J. P.; Klopf, F.; Schäfer, F. *Phys. Rev. B* **2002**, *65*, 195315.
(48) Htoon, H.; Crooker, S. A.; Furis, M.; Jeong, S.; Efros, A. L.; Klimov, V. I. *Phys. Rev. Lett.* **2009**, *102*, 017402.
(49) Sinito, C.; Fernée, M. J.; Goupalov, S. V.; Mulvaney, P.; Tamarat, P.; Lounis, B. *ACS Nano* **2014**, *8*, 11651–11656.
(50) Swarnkar, A.; Chulliyil, R.; Ravi, V. K.; Irfanullah, M.; Chowdhury, A.; Nag, A. *Angew. Chem.* **2015**, *127*, 15644–15648.
(51) Hu, F.; Yin, C.; Zhang, H.; Sun, C.; Yu, W. W.; Zhang, C.; Wang, X.; Zhang, Y.; Xiao, M. *Nano Lett.* **2016**, *16*, 6425–6430.

(52) Galland, C.; Ghosh, Y.; ck, A. S. U.; Hollingsworth, J. A.; Htoon, H.; Klimov, V. I. *Nat. Commun.* **2012**, *3*, 908–7.
(53) Fernée, M. J.; Sinito, C.; Louyer, Y.; Potzner, C.; Nguyen, T.-L.; Mulvaney, P.; Tamarat, P.; Lounis, B. *Nat. Commun.* **2012**, *3*, 1287–1287.
(54) Zhang, C.; Sun, D.; Sheng, C.-X.; Zhai, Y. X.; Mielczarek, K.; Zakhidov, A.; Vardeny, Z. V. *Nat. Phys.* **2015**, *11*, 427–434.